Supporting Information

Efficient separation of $CH_4/C_2H_6/C_3H_8$ enabled by an indium-tetracarboxylate MOF with cross-channel and amino sites

Chaohui He,*[a] Jinglin Guo,[a] Rajamani Krishna,[b] Zhenzhen Jia,[a] Yujuan Zhang,[a] Xiao-Qing Wang*[a] and Tuoping Hu*[a]

[a]*Department of Chemistry, College of Chemistry and Chemical Engineering, North University of China, Taiyuan, 030051, Shanxi, P. R. China*

[b]*Van't Hoff Institute for Molecular Sciences, University of Amsterdam, Science Park 904, 1098 XH Amsterdam, The Netherlands.*

1.1 Materials

All chemicals and reagents were obtained from commercial sources. Ethanol (99.5%), *N,N*-Dimethylacetamide (DMA, AR), HNO_3 (65%), and Indium(III) chloride tetrahydrate ($InCl_3 \cdot 4H_2O$, 99.9%) were obtained from Aladdin. Biphenyl-3,3′,5,5′-tetracarboxylic acid (H_4bptc, 98%) and 4,4′-diamino-[1,1′-biphenyl]-3,3′,5,5′-tetracarboxylic acid (H_4bptc-NH_2, 98%) were purchased from Yanshen Technology Co., Ltd. N_2 (99.999%), CH_4 (99.99%), C_2H_6 (99.99%), and C_3H_8 (99.99%) were used for single-component adsorption.

1.2 Preparation of InOF-12 and NUC-301

InOF-12 was prepared according to a method previously reported in the literature.[1]

NUC-301**:** A mixture of $InCl_3$ (33 mg), H_4bptc-NH_2 (36 mg), DMA (3 mL), ethanol (3 mL), and HNO_3 (240 μL) was placed in a 20 mL glass vial and sonicated for 30 minutes to ensure complete dissolution. The vial was then heated statically at 85 °C in an oven for 5 days. After cooling to room temperature, the resulting product was collected by filtration, washed three times with a mixture of DMA and ethanol, and dried under ambient conditions before final collection. The microcrystalline powder of NUC-301 were obtained in 39% yield based on H_4bptc-NH_2. Elemental analysis (%): Calcd for $C_{16}H_8InN_2O_8$, C 40.8, H 1.71, N 5.95; Found, C 40.61, H 1.93, N 5.18.

1.3 Characterization and equilibrium adsorption experiments

Powder X-ray diffraction (PXRD) characterization of NUC-301 was carried out with a Bruker D8 Advance diffractometer (Cu Kα radiation). The thermal stability of

the samples was assessed via thermogravimetric analysis (TGA), using a NETZSCH STA 449F5 thermal analyzer under a nitrogen (N_2) atmosphere. The temperature was ramped from ambient conditions to 1073 K at a heating rate of 10 K/min. Elemental analysis (C, H, N) was performed using an Elemental Unicube analyzer. Fourier transform infrared (FT-IR) spectra were recorded on a Thermo Fisher Scientific Nicolet iS20 spectrometer. Meanwhile, 77 K N_2 adsorption-desorption isotherms were acquired with a BSD-660 instrument. Before gas sorption analysis, the prepared samples were first subjected to low-boiling-point solvent exchange for 3 days, with the solvent replaced every 12 hours. After the completion of solvent exchange, the samples were treated at 353 K for 12 hours under high-vacuum conditions. The static pure component adsorption isotherms of NUC-301 for CH_4, C_2H_6, and C_3H_8 were measured at a BSD-660 at 288 and 298 K, respectively.

1.4 Isosteric heat of adsorption

The adsorption heat (Q_{st}) is defined as follows:

$$Q_{st} = RT^2\left(\frac{\partial \ln p}{\partial T}\right)_q$$

R is a constant, T indicates the temperature (K), P represents the pressure (kPa) and q is the adsorption amount (mmol/g). These values were calculated using the Clausius-Clapeyron equation based on the single-component adsorption data collected from 0–1 bar at 288 and 298 K, respectively.

1.5 Ideal adsorbed solution theory (IAST) calculations

The single-component adsorption isotherms of CH_4, C_2H_6 and C_3H_8 on NUC-301 obtained at 298 K were fitted using the dual-site Langmuir-Freundlich model.

$$q = q_{A,sat}\frac{b_A p^{vA}}{1 + b_A p^{vA}} + q_{B,sat}\frac{b_B p^{vB}}{1 + b_B p^{vB}}$$

q is the adsorbed capacity per mass of adsorbent (mol/kg), $q_{A,sat}$ and b_A are the saturation uptake capacities and the constant at site A, respectively and P is the total pressure of the gas at the equilibrium (kPa).

The adsorption selectivity defined as follows:

$$S_{ads} = \frac{q_A/q_B}{y_A/y_B}$$

where q_A and q_B represent the component molar loading within the MOFs and y_A and y_B are the corresponding mole fraction used in the feed gas mixture.

1.6 Rietveld refinement for NUC-301

The initial structural model for Rietveld refinement was referenced from the published InOF-12 crystallographic data. The refinement results of NUC-301 were obtained by the Rietveld method implemented in TOPAS software (Table S1, CCDC 2489857).

1.7 Grand canonical Monte Carlo simulations

The GCMC calculations were performed using the Sorption module in BIOVIA Materials Studio (version 8.0) under three-dimensional periodic boundary conditions.[2] The COMPASS force field was employed to describe interatomic interactions. The Ewald method was used to calculate the electrostatic energy, and the van der Waals energy was calculated within a cutoff distance of 12 Å. Each simulation consisted of 2×10^7 equilibration moves followed by 2×10^7 production moves to ensure convergence. Monte Carlo moves included molecular translations and rotations (for non-spherical molecules), as well as insertion and deletion of guest molecules. For gas molecules, LJ parameters for CH_4, C_2H_6 and C_3H_8 were taken from the united-atom TraPPE force field,[3] as summarized in Table S5. GCMC simulations were then performed to study

the adsorption behaviors of CH_4, C_2H_6 and C_3H_8 at 298 K and 1 bar. The primary adsorption sites were identified using the Adsorption Locator module by locating energetically favorable positions of guest molecules within the frameworks. The isosteric heats of adsorption (Q_{st}) were calculated at 298 K using the fluctuation method implemented in the Sorption module.[4]

1.8 Transient breakthrough simulations

Transient breakthrough simulations were carried out for 85/10/5 $CH_4/C_2H_6/C_3H_8$ mixtures at 298 K and 100 kPa using the methodology described in earlier publications.[5-9] In these simulations, intra-crystalline diffusion influences are ignored. The simulations were performed for a breakthrough tube with the following parameters:

Inside diameter of breakthrough tube = 4 mm

Length of packed bed = 120 mm

The flow rates at the inlet, Q_0 = 2 mL min^{-1}

The sample mass of MOF in the packed bed m_{ads} = 0.76 g.

The MOF framework density, ρ = 812 kg m^{-3}.

The mixture adsorption equilibrium were determined using the Ideal Adsorbed Solution Theory (IAST) of Myers and Prausnitz.[10]

The breakthrough data are presented in terms of the dimensionless concentrations at the exit of the fixed bed, c_i/c_{i0}, as function of the modified time parameter

$$\frac{(t = \text{time, min})}{(\text{g MOF packed in tube})} = \frac{t}{m_{ads}} = \text{min g}^{-1}.$$

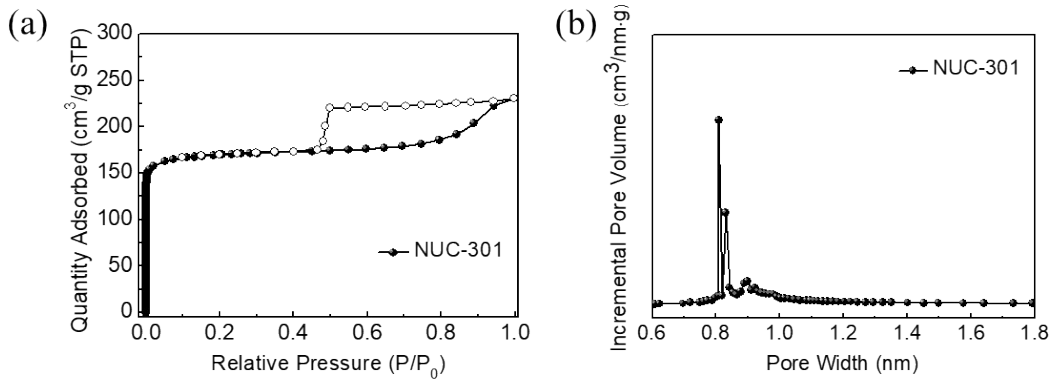

Fig. S1. (a) N_2 adsorption-desorption isotherms of NUC-301 at 77 K. (b) The pore distribution of NUC-301.

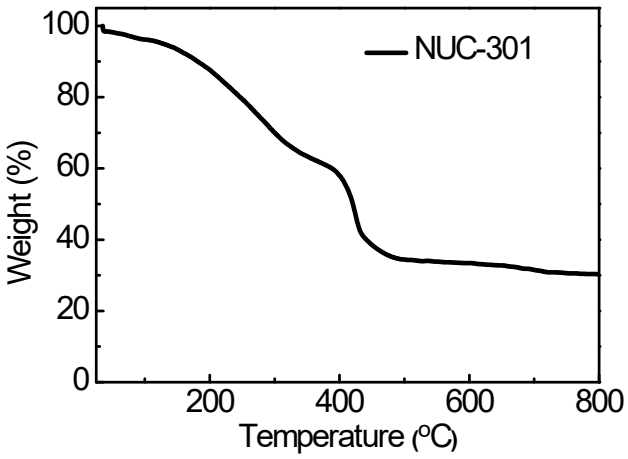

Fig. S2. TGA curves of NUC-301.

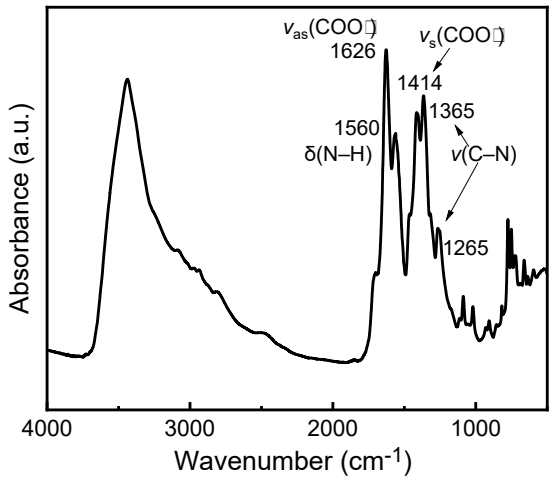

Fig. S3. The FT-IR spectra of activated NUC-301 samples.

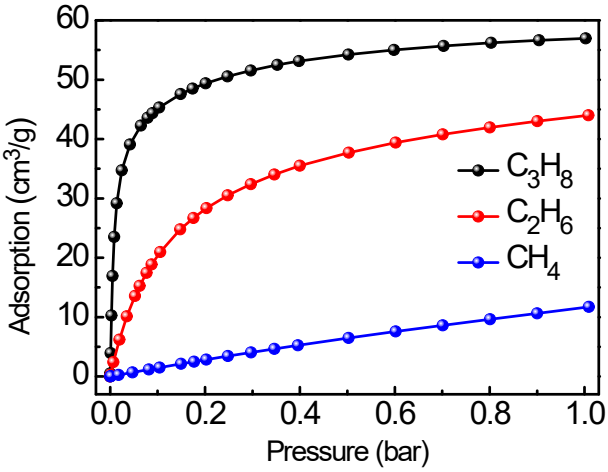

Fig. S4. The single-adsorption isotherms of NUC-301 for CH_4, C_2H_6 and C_3H_8 at 288 K.

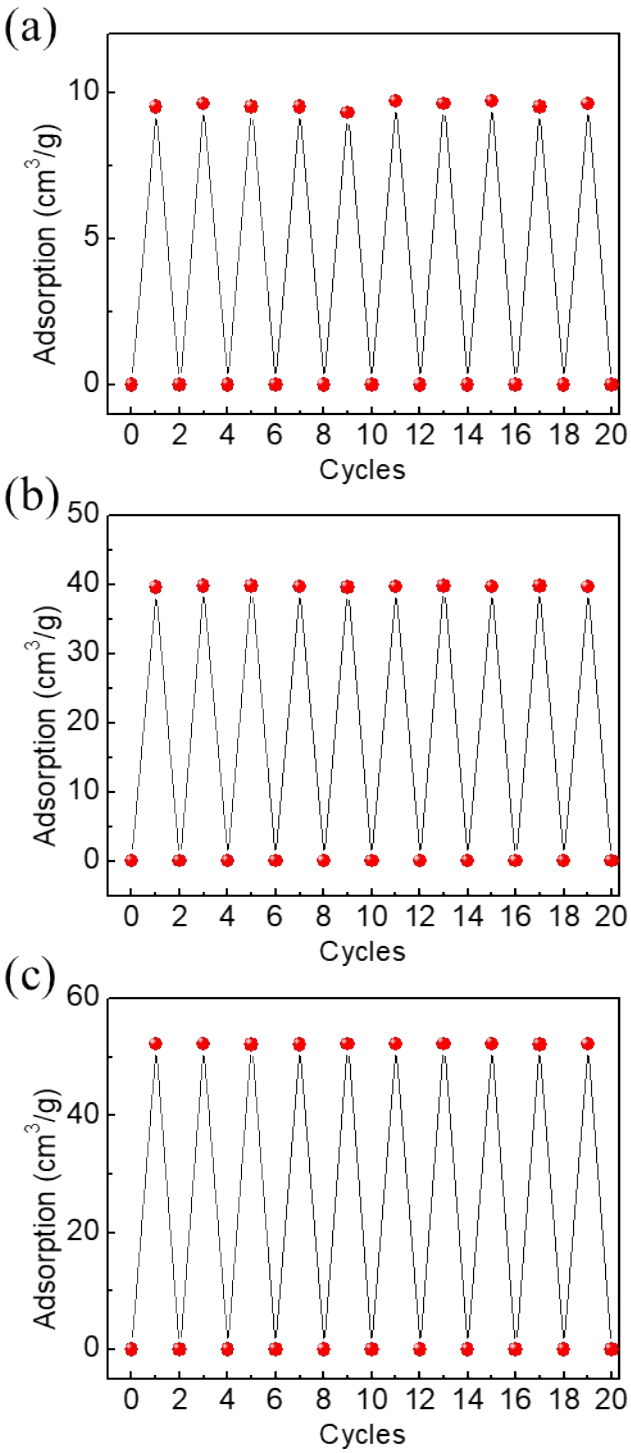

Fig. S5 Cyclic (a) CH_4, (b) C_2H_6, and (c) C_3H_8 adsorption measurements on NUC-301at 298 K and 1 bar.

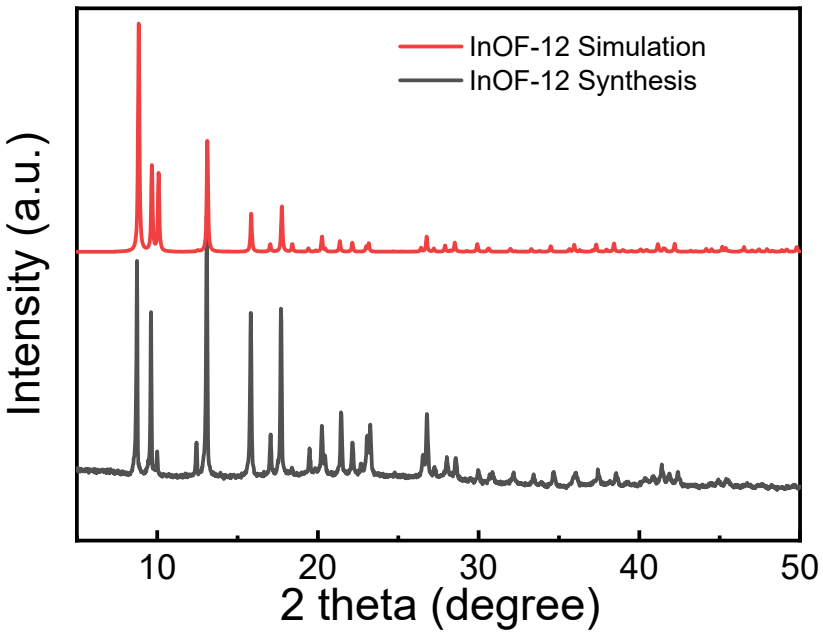

Fig. S6. PXRD patterns recorded for InOF-12.

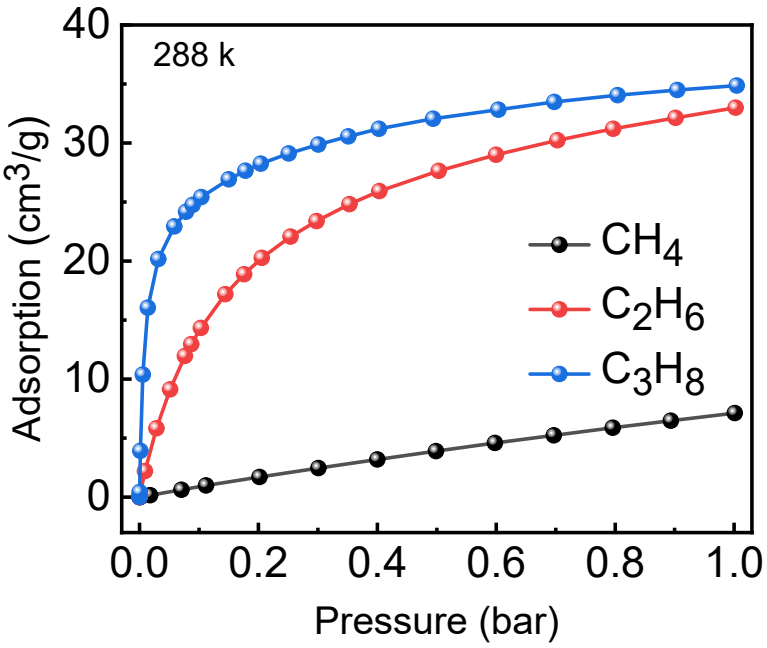

Fig. S7. The single-adsorption isotherms of InOF-12 for CH_4, C_2H_6 and C_3H_8 at 288 K.

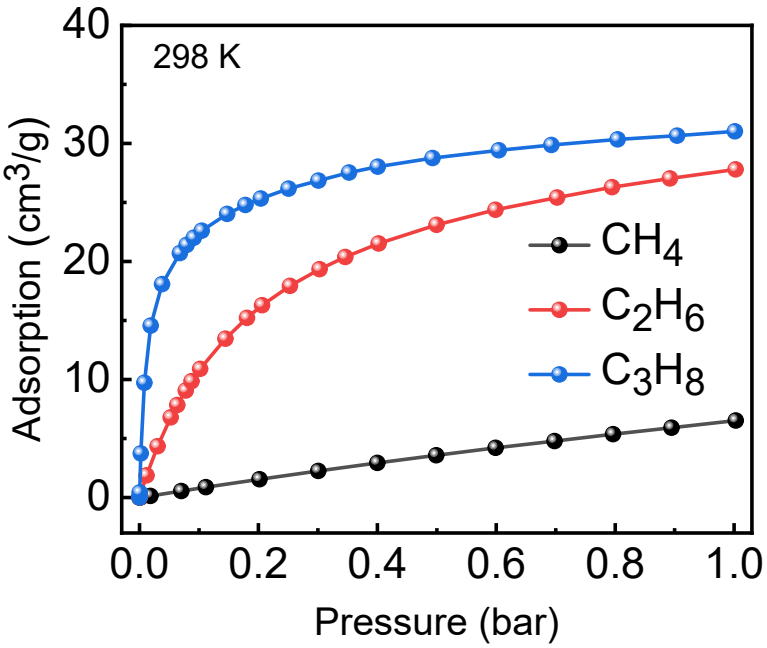

Fig. S8. The single-adsorption isotherms of InOF-12 for CH_4, C_2H_6 and C_3H_8 at 298 K.

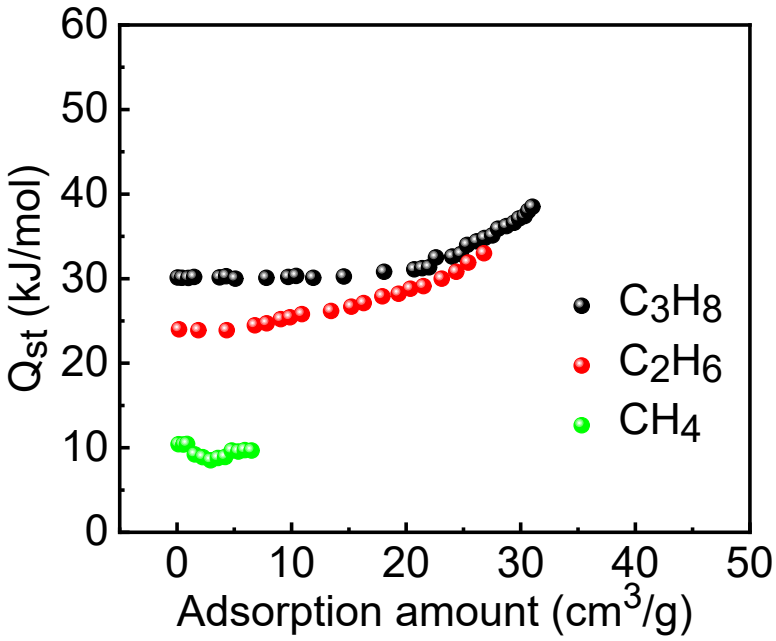

Fig. S9. The adsorption heats of InOF-12 for CH_4, C_2H_6 and C_3H_8.

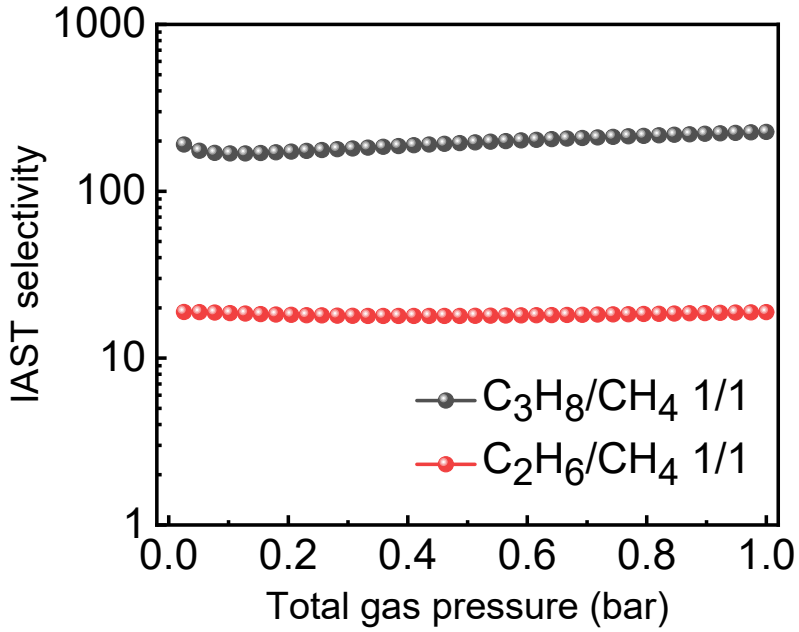

Fig. S10. The adsorption selectivity of C_3H_8/CH_4(1/1) and C_2H_6/CH_4 (1/1) for InOF-12 at 298 K.

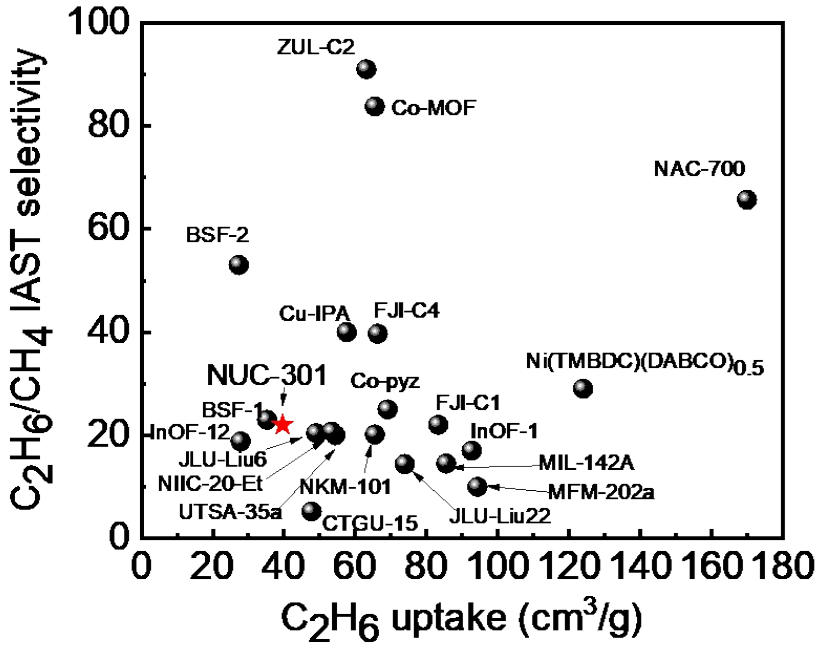

Fig. S11 A comparison of the C_2H_6/CH_4 adsorption selectivity and C_2H_6 uptake for previously reported adsorbents.

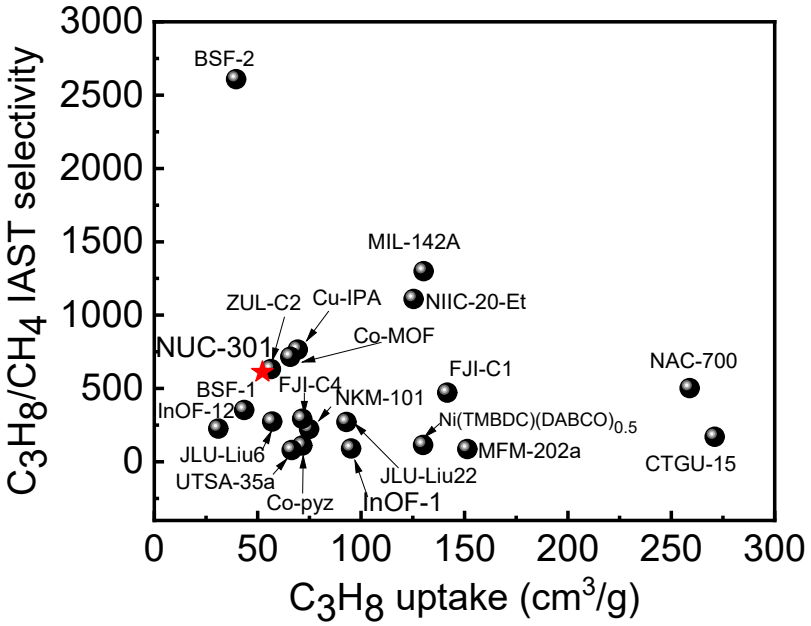

Fig. S12 A comparison of the C_3H_8/CH_4 adsorption selectivity and C_3H_8 uptake for previously reported adsorbents.

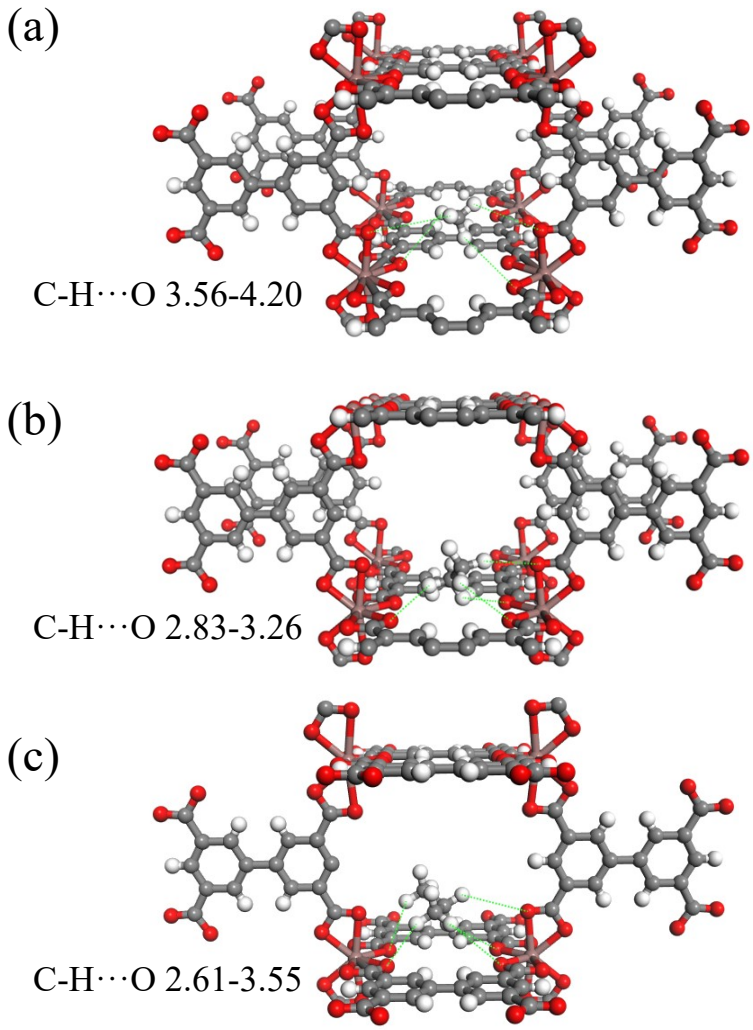

Fig. S13 The main adsorption sites of InOF-12 for (a) CH_4, (b) C_2H_6, and (c) C_3H_8 were identified using GCMC simulations.

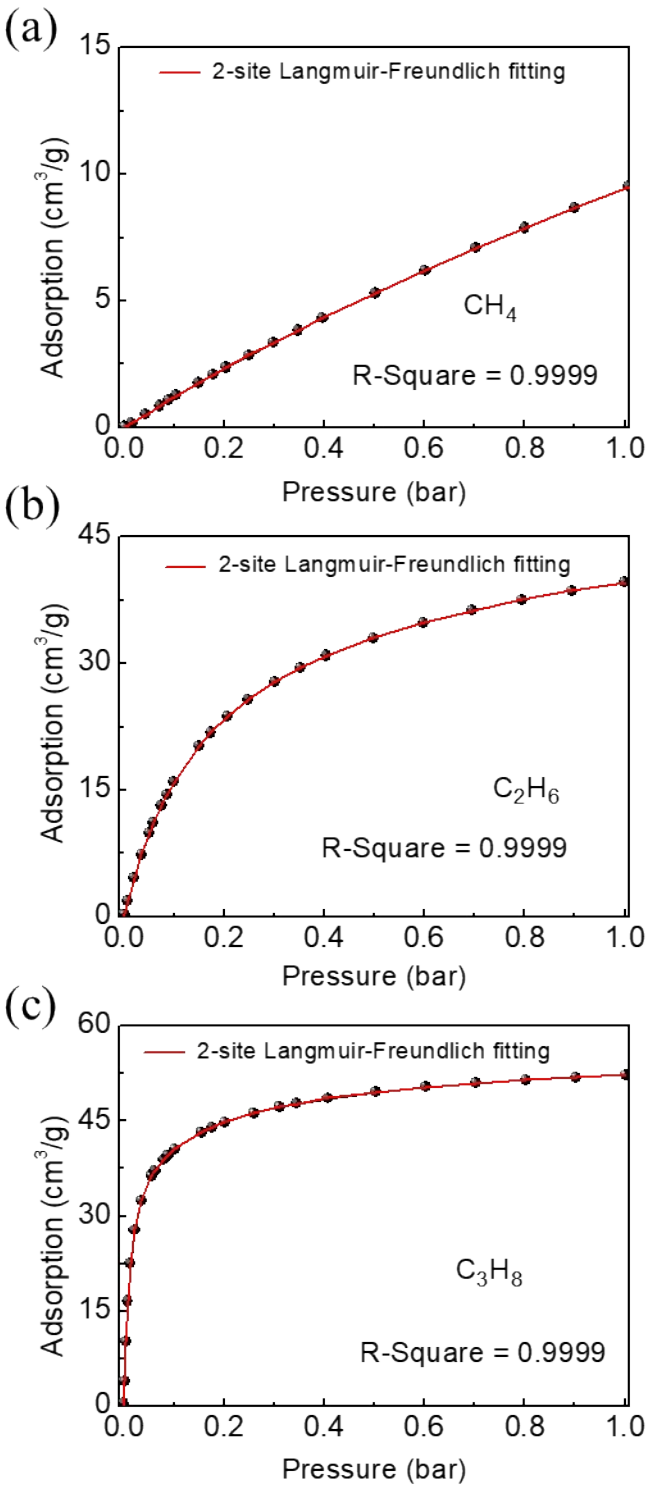

Fig. S14 CH_4, C_2H_6 and C_3H_8 adsorption isotherms at 298 K in NUC-301 with dual-site Langmuir-Freundlich model fits.

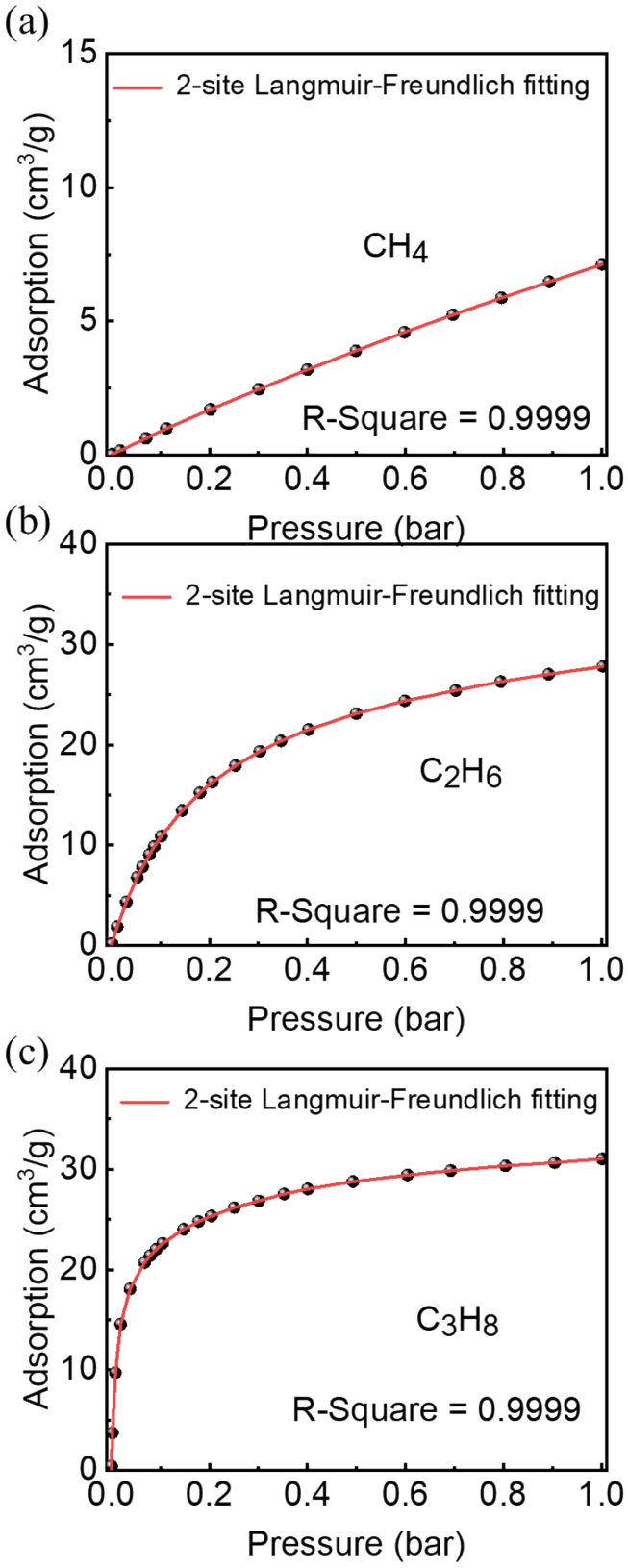

Fig. S15 CH_4, C_2H_6 and C_3H_8 adsorption isotherms at 298 K in InOF-12 with dual-site Langmuir-Freundlich model fits.

Table S1. Main parameters of processing refinement.

compound	**NUC-301**
sp. gr.	P 42/m m c
a (Å)	9.9607
b (Å)	9.9607
c (Å)	18.0472
α (°)	90.0000
β (°)	90.0000
γ (°)	90.0000
V (Å^3)	1790.56
no. of reflection	207
2θ-interval	5°-65°
R_{wp} (%)	6.36
R_p (%)	4.88
R_{exp} (%)	5.46
^{2}	1.17

Table S2 Physicochemical properties of CH_4, C_2H_6 and C_3H_8[11]

	Structure	Molecular size (Å^3)	Kinetic diameter (Å)	Boiling point (K)	Polarizability (×10^{-25}/cm^3)
CH_4		3.70 × 3.70 × 3.70	3.8	111.6	26
C_2H_6		3.81 × 4.08 × 4.82	4.44	184.6	44.3
C_3H_8		4.20 × 4.60 × 6.80	4.9	230.9	62.9

Table S3 Summary of C_2H_6/C_3H_8 adsorption capacities and IAST selectivities (for C_2H_6/CH_4 (1/1) and C_3H_8/CH_4 (1/1) mixtures) of reported MOFs at 298 K and 1 bar

Adsorbents	C_2H_6 (cm^3/g)	C_3H_8 (cm^3/g)	C_2H_6/CH_4 selectivity	C_3H_8/CH_4 selectivity	Reference
Co-pyz	69.1	71.6	25	111	[12]
CTGU-15	47.7	271	5.2	170.7	[13]
JLU-Liu6	49	57	20.4	274.6	[14]
UTSA-35a	54.4	66.5	20	80	[15]
JLU-Liu22	73.9	92.9	14.4	271.5	[16]
MFM-202	94.3	151.4	10	87	[17]
$Ni(TMBDC)(DABCO)_{0.5}$	124	130	29	115	[18]
NKM-101	65.5	74.9	20.1	223.1	[19]
InOF-1	92.7	95.2	17	91	[20]
Cu-IPA	57.6	69.4	40	765	[21]
ZUL-C2	63.1	56.4	91	632	[22]
BSF-1	35.2	43.5	23	353	[23]
Co-MOF	65.5	65.8	83.8	715.6	[24]
NAC-700	170	258.9	65.7	501.9	[25]
FJI-C4	66.3	71.5	39.7	293.4	[26]
FJI-C1	83.3	141.7	22	471	[27]
BSF-2	27.3	39.6	53	2609	[28]
MIL-142A	85.5	130.3	14.5	1300	[29]
NIIC-20-Et	53.4	125.4	20.7	1110	[30]
InOF-12	27.8	31	18.8	226.5	This work

NUC-301	39.6	52.3	22	612	This work

Table S4 A comparison of adsorption performances of NUC-301 and InOF-12 (conditions: 298 K, 1 bar; 1:1 v/v for selectivity; near-zero coverage for isosteric heat).

	NUC-301	**InOF-12**
CH_4 (cm^3/g)	9.5	6.5
C_2H_6 (cm^3/g)	39.6	27.8
C_3H_8 (cm^3/g)	52.3	31
C_2H_6/CH_4 selectivity	22	18.8
C_3H_8/CH_4 selectivity	612	226.5
Experimental *Qst* of CH_4 (kJ/mol)	13.1	10.4
Experimental *Qst* of C_2H_6 (kJ/mol)	26.3	24.1
Experimental *Qst* of C_3H_8 (kJ/mol)	33.8	30.1
Calculated *Qst* of CH_4 (kJ/mol)	16.7	13.7
Calculated *Qst* of C_2H_6 (kJ/mol)	29.5	28.3
Calculated *Qst* of C_3H_8 (kJ/mol)	36.7	33.5

Table S5 Charges and Lennard-Jones parameters of CH_4, C_2H_6 and C_3H_8 molecules.

Atom type	σ (Å)	ε (K)	Charge (e)
CH_4	3.73	148	0
CH_3_C_2H_6	3.75	98	0
CH_3_C_3H_8	3.75	98	0
CH_2_C_3H_8	3.95	46	0

Table S6 Dual-Langmuir-Freundlich fitting parameters for CH_4, C_2H_6 and C_3H_8 in NUC-301 at 298 K.

	Site A			Site B			R^2
	$q_{A,sat}$	b_A	v_A	$q_{B,sat}$	b_B	v_B	
	$cm^3\ g^{-1}$	bar^{-1}	dimensionless	$cm^3\ g^{-1}$	bar^{-1}	dimensionless	
CH_4	29.19	0.28	1.35	4.22	2.69	1.03	0.9999
C_2H_6	27.27	0.63	0.86	32.56	8.18	1.05	0.9999
C_3H_8	20.81	4.12	0.92	35.64	235.12	1.17	0.9999

Table S7 Dual-Langmuir-Freundlich fitting parameters for CH_4, C_2H_6 and C_3H_8 in InOF-12 at 298 K.

	Site A			Site B			R^2
	$q_{A,sat}$	b_A	ν_A	$q_{B,sat}$	b_B	ν_B	
	$cm^3\ g^{-1}$	bar^{-1}	dimensionless	$cm^3\ g^{-1}$	bar^{-1}	dimensionless	
CH_4	23.42	0.31	1.29	2.14	2.88	0.96	0.9999
C_2H_6	32.42	4.66	0.97	358.1	0.003	1.89	0.9999
C_3H_8	20.37	106.63	1.01	14.49	2.91	091	0.9999

References

1. J. Qian, P. Yu, K. Su, Y. Dong, S. Huang and M. Hong, *CrystEngComm*, 2015, **17**, 8512-8518.
2. X.-W. Gu, J.-X. Wang, E. Wu, H. Wu, W. Zhou, G. Qian, B. Chen and B. Li, *J. Am. Chem. Soc.*, 2022, **144**, 2614-2623.
3. M. G. Martin and J. I. Siepmann, *J. Phys. Chem. B*, 1998, **102**, 2569-2577.
4. L. Song, H.-T. Zheng, Z.-Q. Zhou, X.-Y. Zhu, C.-X. Chen, J.-J. Jiang, D. Fenske, X.-H. Xiong, J. Guo and Z.-W. Wei, *Sep. Purif. Technol.*, 2025, 135493.
5. R. Krishna, *Microporous Mesoporous Mater.*, 2014, **185**, 30-50.
6. R. Krishna, *RSC Advances*, 2015, **5**, 52269-52295.
7. R. Krishna, *RSC Advances*, 2017, **7**, 35724-35737.
8. R. Krishna, *Sep. Purif. Technol.*, 2018, **194**, 281-300.
9. R. Krishna, *ACS Omega*, 2020, **5**, 16987-17004.

10. A. L. Myers and J. M. Prausnitz, *AlChE J.*, 1965, **11**, 121-127.

11. J.-R. Li, R. J. Kuppler and H.-C. Zhou, *Chemical Society Reviews*, **2009**, 38, 1477-1504.

12. L. Zhao, P. Liu, C. Deng, T. Wang, S. Wang, Y.-J. Tian, J.-S. Zou, X.-C. Wu, Y. Zhang and Y.-L. Peng, *Nano Res.*, 2023, **16**, 12338-12344.

13. D. Lv, Z. Liu, F. Xu, H. Wu, W. Yuan, J. Yan, H. Xi, X. Chen and Q. Xia, *Sep. Purif. Technol.*, 2021, **266**, 118198.

14. D. Wang, T. Zhao, Y. Cao, S. Yao, G. Li, Q. Huo and Y. Liu, *Chem. Commun.*, 2014, **50**, 8648-8650.

15. Y. He, Z. Zhang, S. Xiang, F. R. Fronczek, R. Krishna and B. Chen, *Chem. Commun.*, 2012, **48**, 6493-6495.

16. D. Wang, B. Liu, S. Yao, T. Wang, G. Li, Q. Huo and Y. Liu, *Chem. Commun.*, 2015, **51**, 15287-15289.

17. S. Gao, C. G. Morris, Z. Lu, Y. Yan, H. G. Godfrey, C. Murray, C. C. Tang, K. M. Thomas, S. Yang and M. Schröder, *Chem. Mater.*, 2016, **28**, 2331-2340.

18. Y. Wu, Z. Liu, J. Peng, X. Wang, X. Zhou and Z. Li, *ACS Appl. Mater. Interfaces* 2020, **12**, 51499-51505.

19. Y. Qiao, X. Chang, J. Zheng, M. Yi, Z. Chang, M.-H. Yu and X.-H. Bu, *Inorg. Chem.*, 2021, **60**, 2749-2755.

20. Y. Chen, Z. Qiao, D. Lv, H. Wu, R. Shi, Q. Xia, H. Wang, J. Zhou and Z. Li, *Ind. Eng. Chem. Res.*, 2017, **56**, 4488-4495.

21. D. Lin, S. Tu, L. Yu, Y. Yuan, Y. Wu, X. Zhou, Z. Li and Q. Xia, *Ind. Eng.*

Chem. Res., 2023, **62**, 5252-5261.

22. J. Zhou, T. Ke, F. Steinke, N. Stock, Z. Zhang, Z. Bao, X. He, Q. Ren and Q. Yang, *J. Am. Chem. Soc.*, 2022, **144**, 14322-14329.

23. Y. Zhang, L. Yang, L. Wang, S. Duttwyler and H. Xing, *Angew. Chem.*, 2019, **131**, 8229-8234.

24. S. M. Wang, L. Xu, L. P. Zhang, Y. T. Li, T. Wang and Q. Y. Yang, *Adv. Funct. Mater.*, 2025, 2504251.

25. J. Wang, R. Krishna, T. Yang and S. Deng, *J. Mater. Chem. A*, 2016, **4**, 13957-13966.

26. L. Li, X. Wang, J. Liang, Y. Huang, H. Li, Z. Lin and R. Cao, *ACS Appl. Mater. Interfaces*, 2016, **8**, 9777-9781.

27. Y. Huang, Z. Lin, H. Fu, F. Wang, M. Shen, X. Wang and R. Cao, *ChemSusChem*, 2014, **7**, 2647-2653.

28. Y. Zhang, L. Yang, L. Wang, X. Cui and H. Xing, *J. Mater. Chem. A*, 2019, **7**, 27560-27566.

29. Y. Yuan, H. Wu, Y. Xu, D. Lv, S. Tu, Y. Wu, Z. Li and Q. Xia, *Chem. Eng. J.*, 2020, **395**, 125057.

30. A. A. Lysova, K. A. Kovalenko, A. S. Nizovtsev, D. N. Dybtsev and V. P. Fedin, *Chem. Eng. J.*, 2023, **453**, 139642.